Numerical and Experimental Investigation of Axial Gap Variation in High-Pressure Steam Turbine Stages

Juri Bellucci[1], Filippo Rubechini[1], Andrea Arnone[1], Lorenzo Arcangeli[2], Nicola Maceli[2], Berardo Paradiso[3], Giacomo Gatti[3]

This work aims at investigating the impact of axial gap variation on aerodynamic performance of a high-pressure steam turbine stage. Numerical and experimental cam-paigns were conducted on a 1.5-stage of a reaction steam turbine. This low speed test rig was designed and operated in different operating conditions. Two different configurations were studied in which blades axial gap was varied in a range from 40% to 95% of the blade axial chord. Numerical analyses were carried out by means of three-dimensional, viscous, unsteady simulations, adopting measured inlet/outlet boundary conditions. Two sets of measurements were performed: steady measurements, from one hand, for global performance estimation of the whole turbine, such as efficiency, mass flow, and stage work; steady and unsteady measurements, on the other hand, were performed down-stream of rotor row, in order to characterize the flow structures in this region. The fidelity of computational setup was proven by comparing numerical results to measurements. Main performance curves and spanwise distributions have shown a good agreement in terms of both shape of curves/distributions and absolute values. Moreover, the compari-son of two-dimensional maps downstream of rotor row has shown similar structures of the flow field. Finally, a comprehensive study of the axial gap effect on stage aerody-namic performance was carried out for four blade spacings (10%, 25%, 40%, and 95%of S1 axial chord) and five aspect ratios (1.0, 1.6, 3, 4, and 5). The results pointed out how unsteady interaction between blade rows affects stage operation, in terms of pressure and flow angle distributions, as well as of secondary flows development. The combined effect of these aspects in determining the stage efficiency is investigated and discussed in detail.

Introduction

The increasingly tighter customers' requirements lead toward the design of machines with higher efficiency, power density, reliability, and reduced costs. In this scenario, one of the parameters which can play a key role is the axial gap between adjacent blade rows, given its close link with the whole turbine length, and with the mechanical and the aerodynamic performance. In fact, this parameter strongly impacts the aerodynamic as well as the mechanical behavior in terms of wake mixing, wake/shock interaction in the case of transonic stages, and the secondary flows effect on the downstream row. Moreover, blade loading and aeromechanical forcing on the downstream row is impacted. Generally, increasing the axial gap reduces the rows interaction. Due to the high stator discharge flow angle, the stator wake is much longer in case of high-gap configurations, thus undergoing considerable mixing before entering the rotor. When the spacing is reduced, the potential interaction significantly alters the picture. Not only are the incoming wakes less diffused due to their reduced free path, but also the interaction alters the flow field in such a way that pressure and flow angle are much more nonuniform. As a result of such nonuniformity, both the stator and the rotor operation can be substantially altered with respect to the design intent.

The research in this area is currently active. In fact, the need for understanding how these mechanisms develop and interact each other has been observed in many experimental and numerical works: the literature on this topic is really wide. In the past, this issue has been faced by using correlative approaches, exploiting empirical or analytical expressions for losses estimation of turbine blades. Generally, these methods do not specifically account for the losses associated with the axial gap, but rather include these losses within the secondary losses. As a consequence, it is not possible to evaluate the single contribution of the axial gap. Furthermore, even when these losses are taken into account separately from the others, often they are overestimated. Nowadays, the main goal is in trying to explain the physical mechanisms through which blade rows interactions alter the flow field and hence the performance [1]. In particular, the attention is focused on mixing losses and secondary flows development [2–4], blade

[1]Department of Industrial Engineering, University of Florence, via di Santa Marta, 3, Florence 50139, Italy

[2]GE Oil & Gas, via Felice Matteucci, 2, Florence 50127, Italy

[3]Dipartimento di Energia, Politecnico di Milano, via Lambruschini, 4, Milan 20158, Italy

Contributed by the Turbomachinery Committee of ASME for publication in the Journal of Engineering for Gas Turbines and Power. Manuscript received August 4, 2016; final manuscript received August 31, 2016; published online January 4, 2017. Editor: David Wisler.

loading modification [5], flow field in the interstage region and downstream of blade rows [6–9], stage performance [10], and on the proper choice of the computational framework to accurately predict these effects [11]. In all these works, as well as in many others, blades aspect ratios are generally low, ranging from 0.7 to 1.5 (2.0 in exceptional case), and Reynolds numbers are low compared to the ones of a real application (from about 3.0×10^5 to 8.0×10^5). On one hand, this choice often depends on the best compromise between test rig layout and Reynolds number that can be obtained. On the other hand, as a matter of fact, these configurations have high secondary flows and enhanced rows interaction, thus they are the best candidates to study all the flow structures previously mentioned. As far as the stage performance is concerned, there is still a sort of uncertainty on the axial gap value that ensures the highest aerodynamic performance, as well as on the shape of efficiency gain trend. Looking for example at the works of Refs. [5], [8], and [10], the maximum efficiency is obtained in a range of axial gap between 20% and 40% of blade axial chord, and the shapes of efficiency gain are quite different. The study of the effect of axial gap between blade rows is an issue that can become very lengthy and costly to be faced experimentally. The high maturity level of computational fluid dynamics (CFD) can play an important role in replacing such campaigns with numerical simulations, which are increasingly fast and reliable. In fact, the development of the numerical codes allows for high-fidelity viscous, three-dimensional unsteady analysis, including many real-geometry details of the machine layout such as shroud leakages, with a good trade-off in terms of time-consumption and model complexity.

This work aims at investigating the impact of axial gap variation on aerodynamic performance of a high-pressure steam turbine stage. After the description of the numerical framework and of the experimental test rig, the fidelity of the computational setup will be proven by comparing numerical results to measurements, in terms of main performance curves, spanwise distributions and two-dimensional flow field maps downstream of the rotor. Finally, a comprehensive study of the axial gap effect on stage aerodynamic performance will be addressed for four blade spacings (10%, 25%, 40%, and 95% of S1 axial chord) and five aspect ratios (1.0, 1.6, 3, 4, and 5). The results of this analysis will be presented and discussed in detail.

Computational Framework

The Flow Solver. All the computations presented in this work were performed using the TRAF code. It is a steady/unsteady, multigrid/multiblock flow solver for the three-dimensional Reynolds-averaged Navier–Stokes equations. A detailed description of the numerical scheme can be found in Arnone [12]. The available turbulence closures are some of the commonly used ones for computations in the turbomachinery industry (e.g., Spalart–Allmaras [13], Wilcox's k–ω [14], and Menter's SST model [15]). The code is recently parallelized for both distributed and shared memory systems, following the trend of high performance computing cluster architectures. The distributed memory parallelization is based on the message passing interface (MPI) standard for communication, while the OpenMP standard was adopted for the shared memory parallelization. These two approaches can be independently selected or combined in a hybrid, master-only OMP-MPI parallelism at the compiling level.

The computational framework is validated against field data to compute transonic/supersonic cascade flows [16,17] as well as stator/rotor interaction in axial turbines [18,19], compressors [20–22], and turbo-expanders [23,24].

Shroud Leakage Model. In shrouded turbines, the leakage flows play an important role in the overall turbine performance. The physics of these secondary flows and their interaction with the mainstream flow have been intensively investigated in recent years (Wallis et al. [25], Pfau et al. [26], Rosic et al. [27]). These studies show that these complex, three-dimensional and nonuniform flows affect the main flow path, modifying the blade loading and pressure distribution near the endwalls. They also change the incidence and enhance the secondary flows in the next blade row, with a consequent rise of the associated losses. As discussed by Rosic et al. [28], the need to account for the leakage flows in a three-dimensional multistage calculation has led to the development of shroud models with varying degrees of complexity and computational costs.

In this work, a simple one-dimensional model of shroud cavity was used (Rubechini et al. [29], [30]). For a specific shroud geometry, the model calculates the leakage mass flow, total enthalpy rise, and change in angular momentum through the cavity and the flow conditions at the interface between the cavity and the mainstream. Following an approach similar to that proposed by McGreeham and Ko [31], the flow through the shroud cavity is completely modeled, and its interaction with the main flow path is calculated by imposing coupled source/sink boundary conditions at the cavity/mainstream interface.

The Choice of Test Geometry

The choice of which geometry to test in an experimental rig is always a trade off between the facility layout and the operating/geometrical aspects the designer would aspire to reproduce. In the framework of this work, the focus was the stage module, thus the goal was in choosing the minimum number of rows which ensures the actual multistage environment. For this reason, a numerical campaign was done, aiming at identifying the minimum number of rows to be tested. Computations were carried out for three configurations, namely 1-, 1.5-, and 2-stage, on a cylindrical flow path using three different back-pressures. In this way, the first stage works in the same conditions in any configuration. In order to save computational costs while ensuring sufficiently accurate results, three-dimensional runs were performed adopting a coarse discretization in spanwise direction and with nonviscous endwalls. The outcome of this analysis is summarized in Figs. 1 and 2, where the spanwise distribution of exit flow angle and the static pressure downstream of the first stage rows are shown. The first stator, as expected, always works in the same way, since the downstream row is able to set the right potential field in any configuration. The picture is different for the first rotor. In the single stage case, obviously, there is no downstream row capable of adjusting the pressure downstream of it. Considering instead the 1.5- and 2-stage cases, it can be observed that the 1.5-stage module is enough to mimic the multirow environment of a real machine: the slight difference in static pressure shown in Fig. 2 is negligible. On the basis of this consideration, it has been chosen to test the 1.5-stage configuration, instead of two stages. This has allowed not only to save time and costs to design and construct the fourth row, but also to find the best compromise in terms of

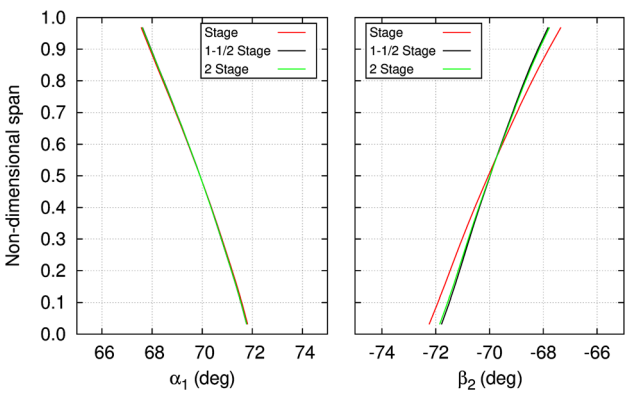

Fig. 1 Spanwise distribution of S1 and *R* exit flow angle

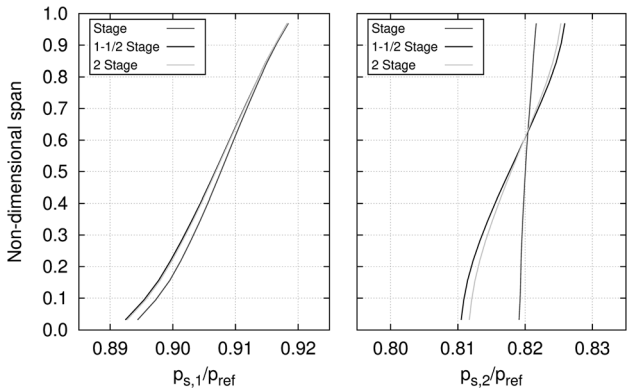

Fig. 2 Spanwise distribution of S1 and *R* nondimensional exit static pressure

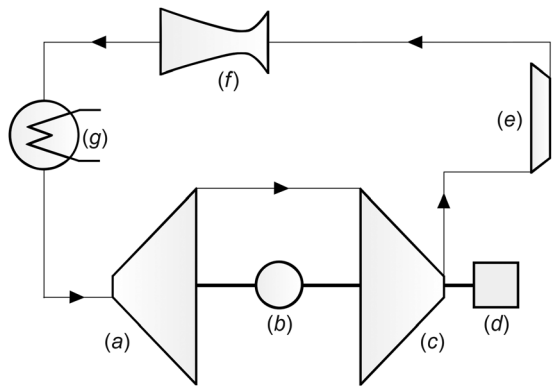

Fig. 3 The low speed closed-loop test rig. Technical scheme and main components: (*a*) turbine stage, (*b*) torque sensor, (*c*) axial compressor, (*d*) DC motor, (*e*) centrifugal blower, (*f*) Venturi nozzle, and (*g*) heat exchanger.

aspect ratio, radius ratio, and Reynolds number, since the axial width of the rig was fixed.

Experimental Test Rig

The test facility is a subsonic closed loop wind tunnel for turbine stages (Fig. 3). The flow rate is provided by a centrifugal blower with variable rotational speed and maximum power of 500 kW. It allows a maximum capacity of 18 m^3/s and a maximum pressure ratio of 1.3. The turbine is braked by a two-stage axial compressor equipped with inlet guide vane (IGV) and variables stator vanes, in order to widen as much as possible the operational range. Compressor and turbine are installed on different shafts, connected through a high accuracy torque-meter. The fine setting of the rotational speed is guaranteed by a DC motor coupled with the compressor shaft. The extra pressure ratio provided by the axial compressor allows a maximum expansion ratio up to 2.1 across the turbine section. Finally, the measurement of the flow rate is performed by means of a calibrated Venturi nozzle. Further details on the design of this facility are provided by Paradiso et al. [32,33].

Test Section and Measurement Setup. The geometry under investigation is representative of an actual 1.5-stage for high/intermediate pressure drums for reaction steam turbines (Fig. 4). The geometrical scale factor between the actual turbine and the test article was 1:1. The flow path is cylindrical and features high aspect ratio (AR $\simeq$ 3, based on rotor chord) and low radius ratio. Rows are composed of prismatic shrouded blades, using the same airfoil geometry for all rows (50% reaction). They experienced a

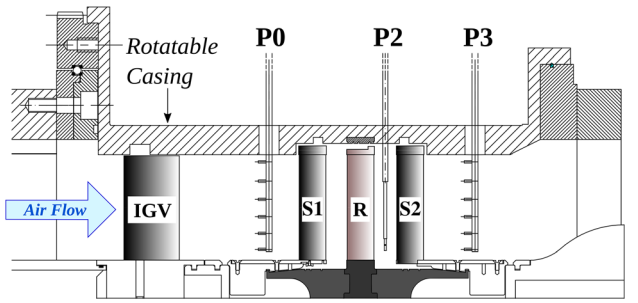

Fig. 4 The test section and the measurement planes of FRAPP probe (plane P2) and rakes (planes P0 and P3). The tangential traversing is obtained by rotating the external casing.

Table 1 Experimental conditions

Inlet total pressure	1.0–1.25 bar
Inlet total temperature	290–310 K
Pressure ratio ($p_{t,0}/p_{s,3}$)	1.05–1.45
Blades is. exit Mach	0.20–0.40
Reynolds	1.5×10^5 to 3.5×10^5
Rotational speed	2000 and 3000 RPM
Turbulence intensity	Low

Table 2 Measurement uncertainty

Total and static pressure	$\pm$0.3%
Total temperature	$\pm$0.1%
Yaw angle	$\pm$0.25 deg
Pitch angle	$\pm$0.30 deg

Zweifel number of about 0.8 and a flow deflection of about 80 deg. S1 and S2 have the same blade count, while the blade count ratio is about 1.13. The stage was arranged in two configurations which differ in the blades axial gap: 40% (hereafter referred to as "nominal" gap) and 95% (hereafter referred to as "large" gap) of S1 axial chord. The second configuration has such a high gap in order to ensure sufficient room for interstage measurements. In order to mimic the repeating stage environment, in which these stages usually are employed, blade rows are preceded by an inlet guide vane (IGV) row. The IGV and the stators are mounted on the inner part of the machine, rather than being hung to the external casing, which is rotatable. This solution allows the investigation of the flow field over the entire annular channel, and the tangential traversing of probes between the rows while keeping the same IGV - S1 - S2 clocking positions.

For each axial gap, measurements were performed at two rotational speed, 2000 and 3000 RPM, and for several pressure ratios, in order to draw a complete loading curve of the stage. A summary of experimental conditions and measurement uncertainty is reported in Tables 1 and 2. As far as the measurement setup is concerned, two different branches of investigation have to be discerned. The first is focused on the performance measurements, and it is based on steady probes (provided by Oil&Gas Technology Laboratory of Florence, Florence, Italy) applied at the inlet (Plane 0) and at the outlet (Plane 3) of the test section. In each of these sections, there are three rakes of Kiel sensors for the total temperature, one rake of Kiel sensors for the total pressure and one rake of three-hole probes for the flow angle. The second branch, instead, focuses on the characterization of the unsteady aerodynamics downstream of the rotor, and relies on the use of a fast response pressure probe. The next paragraph provides more details about the probe, as well as about the data reduction techniques applied.

The FRAPP Probe and the Data Reduction Techniques. The fast response aerodynamic pressure probe (FRAPP) used in this campaign was designed in Politecnico di Milano [34], and was already successfully used in other research scenarios [35,36]. It is essentially a miniaturized single-sensor cylindrical probe, operated as a virtual multihole probe. The pressure readings, therefore, are taken sequentially as the stem rotates around its axis. A total of 5 stem rotations are considered, spaced by 45 deg, where the central one corresponds to the mean rotor swirl angle, which is known from previous investigations. Each acquisition lasts for 1 s, and the sampling frequency is set at 1 MHz. Along with the pressure signals, a $1 \times$ Rev trigger signal is acquired, in order to be able to phase-align the data during the postprocessing. Finally, the measurement plane consists of 50 radial points and 10 circumferential points, covering a full stator pitch. The first step of the classical treatment for unsteady data is the so-called triple decomposition

$$q(t) = \bar{q} + \langle q(t) \rangle + q'(t) \tag{1}$$

where $q(t)$ is a generic signal, $\bar{q}$ is its time average, $\langle q(t) \rangle$ represents the purely periodic component and, finally, $q'(t)$ denotes the random fluctuations. Using the information provided by the trigger signal, it is possible to align every signal to the same rotor phase, and then to perform an ensemble average. This procedure returns the following quantity:

$$\tilde{q}(t) = \bar{q} + q'(t) \tag{2}$$

This means that the unsteadiness unrelated to the rotor rotational frequency is suppressed. After this treatment, the evolution of the flow field can be visualized as a sequence of snapshots, each one related to a specific rotor phase. Finally, since the visualization of a wider plane (with respect to the single stator pitch acquired) can enhance the comprehension of the flow structures, an extension algorithm was implemented. This was necessary in order to take into account the phase-lag introduced by the different blade count of the rotor and the stators.

Assessment of Numerical Setup

Prior to face the issue of axial gap variation, the fidelity of computational setup was proven by comparing numerical results to measurements.

All the numerical results reported hereafter came from three-dimensional, viscous, unsteady computations, adopting phase-lagged boundary conditions [18], allowing to significantly reduce the computational costs, and Wilcox's k–ω model as turbulence closure. A switching RMS residual value ten times lower than the single precision machine zero was considered, resulting in about 5–10 subiterations per time step. As far as the time-averaged performance computation is concerned, efficiency as well as loss coefficients were defined considering the time-averaged mass–weighted total enthalpy and entropy, and work-averaged total pressure [37–39]. To accurately resolve blade rows interaction and secondary flows development, attention was paid to select time-sampling and rows discretization. Time-sampling was imposed considering the trade-off between accuracy and computational costs. The number of time-steps was selected after a sensitivity analysis carried out using three different values: 25, 50, and 100. Fifty time-steps per blade passing period ensured the independence of the solutions from time-steps. Rows discretization was done by means of O-H-type grids with a y^+ value lower than 1 and using 160 cells in the spanwise direction, resulting about 14×10^6 cells overall. The computational mesh used for the large gap configuration is shown in Fig. 5. Finally, spanwise distribution of measured p_t, T_t, and α, at plane P0, and p_s, at plane P3, is adopted as boundary conditions for the computations.

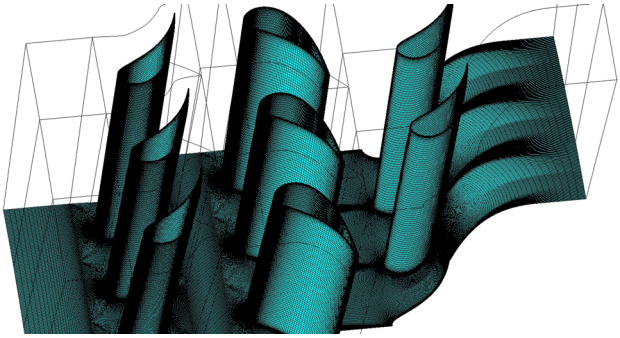

Fig. 5 Computational grids for the large axial gap

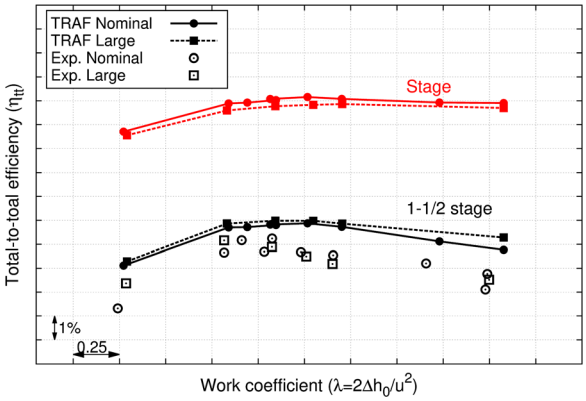

Fig. 6 Efficiency versus work coefficient. Numerical (lines and filled symbols) and experimental results (open symbols) for nominal and large axial gap.

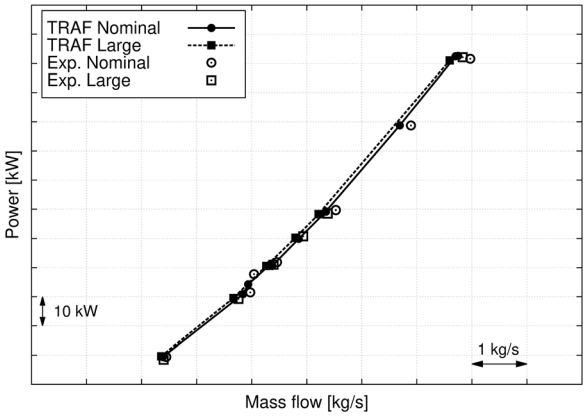

Fig. 7 Power output versus mass flow. Numerical (lines and filled symbols) and experimental results (open symbols) for nominal and large axial gap.

Main Performance. First of all, a comparison of main performance prediction was addressed. Measurements were available in terms of total-to-total efficiency (η_{tt}), work coefficient (λ), power output, and mass flow of the whole turbine, for both nominal and large gap configurations. Results are presented for the 2000 RPM case only. Figures 6 and 7 show the comparison in terms of efficiency trend and loading curve, respectively. The general comment is that numerical and experimental results are in good agreement, with errors within the experimental uncertainty. As far as efficiency trend is concerned, the shape of the curve is typical for this type of blading. A wide and flat high efficiency region is observed near the design point, together with a good off-

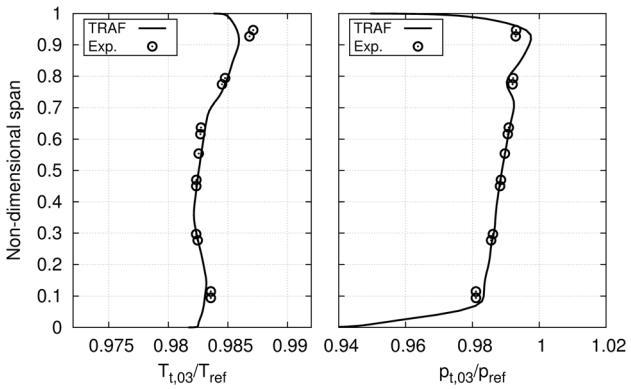

Fig. 8 Spanwise distribution of total temperature and pressure at plane P3: time-average numerical and experimental results (near peak efficiency)

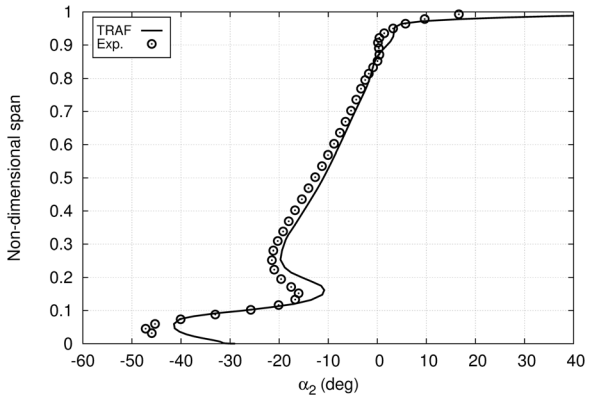

Fig. 9 Spanwise distribution of absolute exit flow angle downstream rotor row: time-average numerical and experimental results (large gap)

design behavior. Computations predict the same shape of the experimental curve and even absolute values are estimated within a tolerance of 1%. Moreover, both results show no or negligible difference in terms of efficiency (about 0.05%) between nominal and large axial gap. In the same plot, CFD results of stage performance are shown. Comparing this curve with the one of whole turbine, it can be observed that they have the same shape, but now, the nominal gap configuration held a constant efficiency gain of about 0.15%, by varying the operating conditions.

Finally, a comparison of spanwise distribution measured at plane P3 is reported in Fig. 8, for total temperature and pressure. For conciseness, only the results of an operating point near peak efficiency are shown. CFD results fit very well with experimental measurements along the whole span, which suggests the right prediction of losses and work exchange of the whole turbine. The only aspect to discuss could be the different trends of total temperature near endwalls. The opposite trend of measurements with respect to calculations would suggest the presence of a heat transfer issue. However, the overall comparison suggests a negligible effect of this aspect on the results.

Flow Field Downstream Rotor. Since the focus of the present work is the effect of blade axial gap on stage performance, the fidelity of computational setup is proven comparing results with measurements downstream of rotor row. Time-averaged and unsteady measurements were available for comparison purposes at 0.5 $C_{ax,R}$, for the large gap configuration only. Unsteady measurements were carried out in the absolute reference frame and

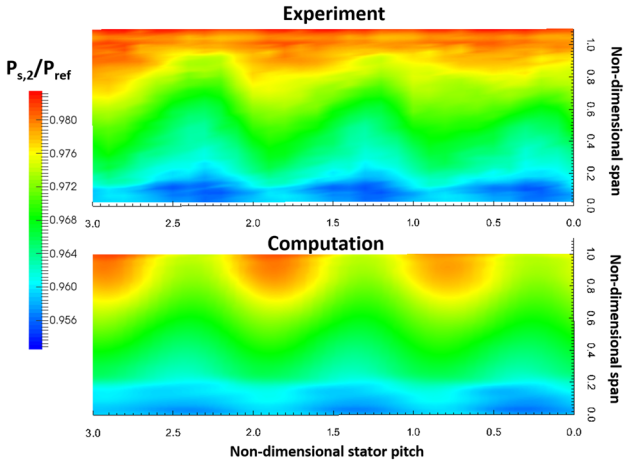

Fig. 10 Static pressure contours downstream rotor row: instantaneous numerical and experimental results for three stator pitch (large gap)

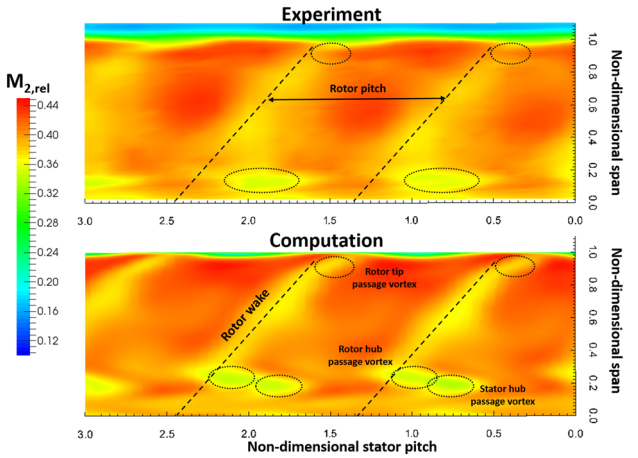

Fig. 11 Relative Mach number contours downstream rotor row: instantaneous numerical and experimental results for three stator pitch (large gap)

with probes aligned to S2 leading edge. Results are presented for the 3000 RPM case only.

A first comparison is reported in Fig. 9, where the time-averaged spanwise distribution of absolute exit flow angle is shown. As general comment, a good agreement between computations and experiments is observed along the whole span. The figure allows to highlight qualitatively the secondary flows structures resulting from the stator/rotor interaction, and the effect of leakage flow at blade tip. Secondary flows have a higher intensity in the hub region, where the penetration along blade height reaches 25% of the span, and flow over/under turning is about 10 deg. Lower impact is observed in the tip region, where the superimposed effect of leakage flows in increasing the exit flow angle is observed.

Figures 10 and 11 show instantaneous contours of static pressure and relative Mach number on three stator pitch. With respect to calculations, experiments span from 0.02 to 1.1, indeed, experimental layout allows to perform interstage measurements in the shroud region. The comparison of static pressure contours highlights a general agreement of the shape of potential field, hence the pressure gradient downstream of rotor. In particular, high and low pressure regions are identified in the same positions and correspond to a stator's pressure modulation since their periodicity is one stator pitch. Some differences appear in the shape of the high

pressure region, which are very well defined in the CFD results with respect to measurements.

Relative Mach number contours allow to highlight the details of the flow field downstream of the rotor. Looking first at computational results, in Fig. 11, the tilted low velocity and high loss region corresponds to the trace of rotor wake. Moreover, another, wide, low velocity region can be identified at about 20% of the span. This is the outcome of the interaction between S1 secondary flows with the rotor ones. The rotor passage vortex can be seen, close to the wake on the suction side, and the trace of passage vortex of the upstream row. Indeed, these two flow structures have a periodicity that meets rotor pitch (the first one) and stator pitch (the second one), respectively. Smaller secondary flow structures are observed in the tip region, where the rotor passage vortex can be seen. These results well agree with the spanwise distribution of absolute flow angle of Fig. 9. As for the others comparison, a general agreement is observed between experiments and computations. The same main flow field structures are recognized in both results, even if numerical ones outline them with more precision. In fact, the passage vortices, highlighted in the computation, are glued in a single wide low velocity region at hub, relatively far from rotor wake. And the tip vortex is less evident due to the stronger interaction with leakage flow.

Overall, the comparison shows an encouraging agreement between CFD and measurements in main performance prediction as well as accurate estimation of flow field structures. In light of this, numerical setup was selected to study the impact of axial gap on stage performance.

Axial Gap Effect on Stage Performance

A comprehensive study of the axial gap effect on stage aerodynamic performance was carried out for four blade spacings (10%, 25%, 40%, and 95% of S1 axial chord) and five aspect ratios (1.0, 1.6, 3, 4, and 5). Blades geometry and flow conditions were the same tested during the experimental campaign previously described. The aspect ratio variation was carried out by varying the blade height at a fixed chord length, thus preserving the Reynolds number. In order to compare all the results in a homogeneous manner, all the computations reported hereafter were performed using uniform inlet boundary conditions, and not the ones measured during the experimental campaign. For all the configurations, computations were performed in three operating conditions around the peak efficiency.

The effect of axial gap variation will be addressed for the AR = 3 case, then the results will be extended to all the cases. First of all, the impact on stage operation is discussed, focusing on two-dimensional flow features, associated with blade-to-blade phenomena. As already said in the introduction, the axial gap

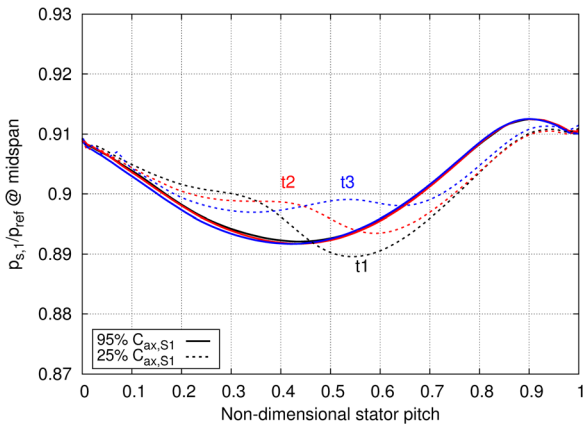

Fig. 12 Static pressure distribution at S1/*R* interface at midspan: effect of blade spacing (instantaneous CFD results, AR = 3)

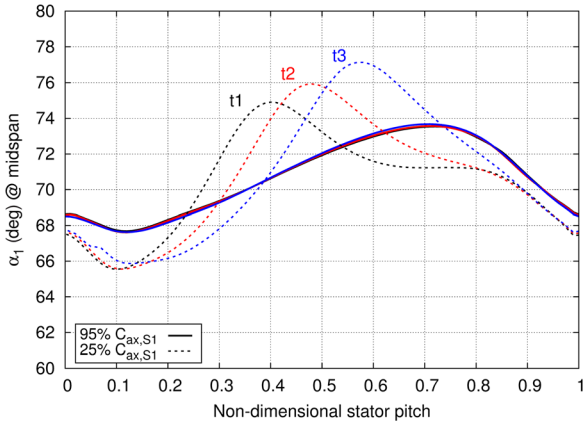

Fig. 13 Absolute exit flow angle distribution at S1/*R* interface at midspan: effect of blade spacing (instantaneous CFD results, AR = 3)

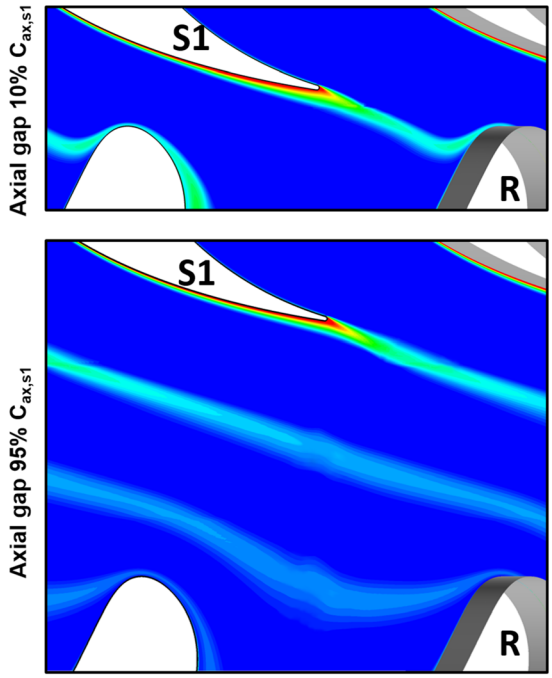

Fig. 14 Entropy contours at stator/rotor interface (S1/*R*): instantaneous numerical results for two extreme axial gap

variation modifies potential interaction, which translates in an alteration of the pitchwise distribution of static pressure and flow angle, and hence of the blades operation. To highlight this, Figs. 12 and 13 show the instantaneous pitchwise distributions of static pressure and blade-to-blade flow angle at stator/rotor interface, at three time instants. For the sake of conciseness, only midspan results for two of the four cases studied are presented. As it can be readily seen, distributions for the reduced axial gap are more nonuniform in space and time, and therefore the operation of downstream rotor vanes differs from one another, depending on the relative position with respect to the stator. The low-subsonic Mach number experienced by these types of blades leads to a pressure nonuniformity lower than the flow angle one. In fact, the last one in corresponding cases almost doubles its variation along a stator pitch for the lower gap. As a result of this nonuniformity, the reduction of blade spacings increases profile loss of both rows, while leading to a lower wake diffusion and mixing before entering downstream row (Fig. 14). For the closest configurations, another important aspect of the time-varying, potential interaction

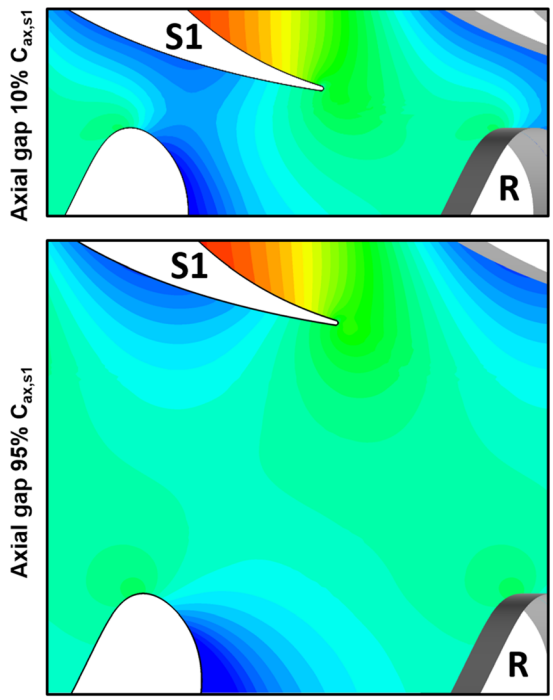

Fig. 15 Static pressure contours at stator/rotor interface (S1/*R*): instantaneous numerical results for two extreme axial gap

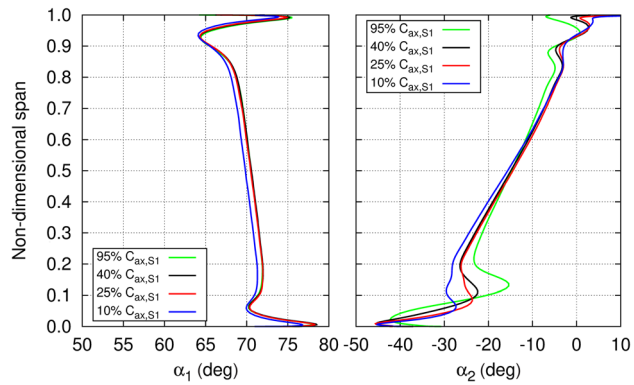

Fig. 16 Spanwise distribution of absolute exit flow angle downstream S1 and *R* row: effect of blade spacing (time-average CFD results, AR = 3)

is that the suction surface of the vane trailing edge and the rotor leading edge can form an effective throat in some relative positions, thus leading to a periodic motion of a low pressure region that is the main responsible for the alteration of stator blade loading and hence of the profile losses. Figure 15 highlights this phenomenon.

As far as secondary flows are concerned, as well illustrated by Sharma et al. [40], their generation mechanisms, especially at the hub, are strongly influenced by the upstream circumferential distortions, such as the wakes of the preceding stator. It is worth noting that the periodic variation in size and strength of the secondary vortices, observed experimentally, equated to almost 40% variation in the rotor secondary losses. In the present case, to catch the impact of axial gap variation on secondary flows, one can look at the time-averaged solution downstream S1 and R rows. Figure 16 shows the time-averaged spanwise distribution of absolute exit flow angle downstream of the stator and rotor row. Looking at the figure, on the stator row, the effect on secondary flows development is limited. In fact, for the smaller axial gap only, the high potential interaction modifies the mean solution,

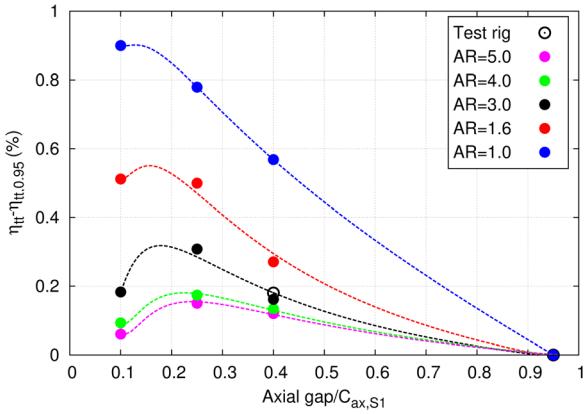

Fig. 17 Stage total-to-total efficiency gain for several axial gap and aspect ratio: CFD results near peak efficiency for Re = 0.3 × 10^6

and, as a consequence, the behavior in the endwalls region. Different are the conclusions for the rotor row. The reduction of blade spacings inhibits the development of stator secondary flows in the interstage space, even if it enhances the flow nonuniformity. The resulting effect is a progressive reduction of secondary flows penetration along blade height downstream of the rotor with decreasing axial gap, which reflects on stage efficiency. In this case, the impact is stronger at blade hub, while tip sections undergo a reduced effect. Walraevens et al. and Restemeier et al. [6,41] found the same effect in their works.

Looking at Fig. 17, it can be observed how the combined effect of flow nonuniformity and secondary flows affects the stage efficiency. Here the total-to-total efficiency gain with respect to the value at axial gap of 95% is reported. Results are presented for all five aspect ratios considered. Filled symbols represent the results obtained in the numerical campaign carried out with uniform boundary conditions, while the open symbols refer to the results obtained in the test rig environment. Dashed lines are shown to qualitatively indicate trends.

First of all, it is important to highlight that for AR = 3 results well agree with the one found in the test rig environment, thus indicating that the use of uniform boundary conditions does not alter the picture. Similar trends are observed for all aspect ratios. Starting from the highest axial gap, approaching the blade rows causes an increase in efficiency. As previously discussed, the main effect is due to a lower interaction and development of secondary flows within the rotor row, together with a reduction of mixing and endwall viscous losses. Due to the relatively high distance between the blade rows, it is likely that profile loss variation plays a role of minor importance on global performance. This statement is true until axial gap reaches values around 15–20% of axial chord. In fact, when the blades become too close to each other, the significant alteration of potential field in the interstage region modifies the stage operation in such a way that it becomes an important source of losses for the stage. As an outcome, the global effect is a reduction of efficiency gain. As far as the impact of aspect ratio variation is concerned, the main effect is to modify the role played by secondary flows growth on stage performance. From Fig. 17, a reduction of AR brings to an increase of the gain up to 0.9% in stage efficiency, without significantly altering the shape of the curve. At the same time, the position of maximum gain slightly shifts toward lower axial gap increasing aspect ratio.

Starting from these results, an attempt is made to quantify the contribution of blade-to-blade phenomena and of secondary flows to the efficiency gain. If it is assumed that endwalls viscous losses are included within secondary losses, the comparison between the gain obtained for AR = 4 and AR = 5 cases indicates that the 1.5 tenth of gain (at maximum) of AR = 5 case can be attributed to potential and mixing losses only. In fact, it is reasonable to

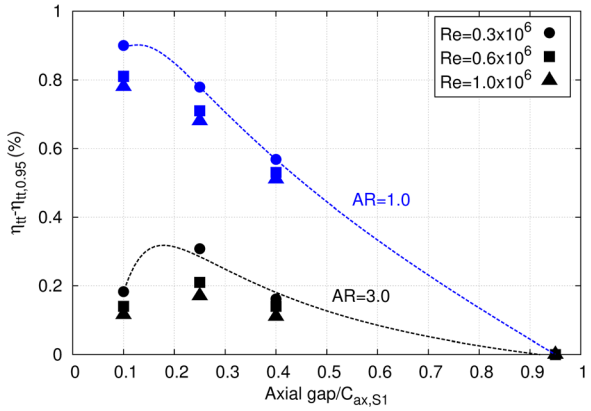

Fig. 18 Stage total-to-total efficiency gain for several axial gap and Reynolds number: CFD results near peak efficiency for AR = 1.0 and AR = 3.0

assume that secondary flows of a configuration with AR = 5 play a little effect on main performance. This result well agrees with the two-dimensional outcomes of Venable et al. and Restemeier et al. [5,41] in terms of absolute value. They found an efficiency variation of about 0.2–0.3%, even if in these works the position of maximum gain is located at higher axial gap. Higher efficiency gains are expected in case of transonic stages, in which the interaction is strengthened by shock waves. In fact, the same authors found in these cases a maximum efficiency penalty around 1% for the closest configuration [1]. In light of all these considerations, when reducing AR, the enhanced efficiency variation with axial gap has to be attributed to the modification of the way in which secondary flows grow and propagate downstream. Overall, the results of Fig. 17 fit the findings obtained by others authors. The efficiency gain for AR = 1 agrees quite well with the outcomes of Venable et al., Gaetani et al., Yamada et al., and Dring et al. [5,8,10,42] in terms of absolute value of efficiency gain, even if the geometry and the operating conditions investigated are quite different. Some discrepancies arise if it is considered the position of maximum gain. In fact, they found the maximum gain position around the 25–40% of axial gap, while in this work it is located approximately in a range of axial gap between 10 and 15%.

Generally real machines applications exhibit a higher Reynolds than the one used to obtain the results of Fig. 17 (about $\mathrm{Re} = 0.3 \times 10^6$). This aspect could lead to a wrong estimation of the role of profile losses and of mixing process in determining stage performance when the axial gap is changed. In fact, it is well-known that mixing process is a phenomenon strongly dependent on the Reynolds number, in particular within laminar-to-turbulent transition region. Even if the computations reported in this work are in fully turbulent conditions, a verification of the effect of the Reynolds number variation was performed for two aspect ratios, 1.0 and 3.0. The results are summarized in Fig. 18, where the same data of Fig. 17 are compared with the new results for two higher Reynolds numbers, that is $\mathrm{Re} = 0.6 \times 10^6$ and $\mathrm{Re} = 1.0 \times 10^6$. The main outcome is that increasing the Reynolds number does not change the shape or the position of the maximum of the curves, while it slightly reduces the efficiency gain (within one-tenth of point) independent of the aspect ratio. The reduction of profile losses and the augmentation of stage efficiency, as a consequence of the Reynolds number increase, change the relative weight of each source of loss involved, which translates in the reduction of the efficiency gain. In fact, the main differences arise in the region of the axial gap around maximum efficiency gain, where profile losses play a key role in determining the stage performance. The effect of Reynolds number vanishes when approaching $\mathrm{Re} = 1.0 \times 10^6$, which is typical of actual machines.

All these considerations emphasize the importance of accounting for the aspect ratio when choosing the axial gap of a turbine stage. This is, in particular, in case of low/medium aspect ratio blades, because of its impact on efficiency.

Summary and Conclusions

This work aims at investigating the impact of axial gap variation on aerodynamic performance of a high-pressure steam turbine stage.

A numerical and experimental campaign was conducted on a 1.5-stage of a reaction steam turbine representative of a real machine layout (full scale). Two different configurations were analyzed by varying blades axial gap: 40% (nominal gap) and 95% (large gap). Three-dimensional, viscous, unsteady simulations were carried out adopting measured inlet/outlet boundary conditions. Two sets of measurements were available for comparison purposes. The first one was focused on performance measurements, and is based on steady probes applied at the inlet and at the outlet of the test section. The second set focuses on the characterization of the unsteady aerodynamics downstream of the rotor, and relies on the use of a fast response pressure probe. The comparison of these data with numerical results has proven the capability of the computational setup to accurately predict main performance as well as the flow field structures downstream of the rotor row.

Once the computational framework was chosen, a comprehensive study of the axial gap effect on stage aerodynamic performance was carried out for four blade spacings (10%, 25%, 40%, and 95% of S1 axial chord) and five aspect ratios (1.0, 1.6, 3, 4, and 5). The results have pointed out how unsteady interaction between blade rows affects stage operation, in terms of pressure and flow angle distribution, as well as secondary flows development. The combined effect of these two aspects together with the mixing and endwalls viscous losses determines stage efficiency. Which of these aspects prevails over the other, affecting stage efficiency, strongly depends on the axial gap value. At first, a reduction of axial gap is associated with an increase of efficiency, due to a lower intensity of secondary flows and to the reduction of endwall and mixing losses. Then, when the rows are too close, wakes and potential interaction become the major source of losses and the stage efficiency starts to drop. These mechanisms are still valid when varying the aspect ratio. The differences lie in the way in which secondary flows grow and propagate downstream, causing an efficiency gain variation up to 0.9%. Higher values are expected toward smaller values of AR.

Finally, the finding of this work emphasizes the importance of accounting for the aspect ratio when choosing the axial gap of a turbine stage. It is worth noticing that these results are strongly dependent on the stage operating conditions. Indeed, all those aspects which could lead to an alteration of rows interaction could change the picture, such as wake/shock interaction, a different blade count ratio, or the effect of impinging wakes on the transitional behavior. However, some of the physical mechanisms involved in the variation on axial gap are identified and can be useful for the designer to address the aerodynamic design of the stage.

Acknowledgment

The present research was carried out in the framework of a joint activity involving both industry and university members. The authors would like to thank GE Oil&Gas for permission to publish this work.

Nomenclature

AR = aspect ratio = H/C
C = chord
h = enthalpy
H = blade height

N = blade count
p = pressure
Re = Reynolds number, $\mathrm{Re} = v_2 C_{\mathrm{rotor}}/\nu$
R = rotor row
S1 = first stator row
S2 = second stator row
T = temperature
u = blade speed
v = velocity magnitude

Greek Symbols

α = absolute flow angle (from axial direction)
β = relative flow angle (from axial direction)
η = efficiency
λ = work coefficient $= 2\Delta h_0/u^2$
ν = kinematic fluid viscosity

Subscripts

ax = axial direction
ref = reference value
s = static
t = total
tt = total-to-total
1 = first stator exit
2 = rotor exit
3 = second stator exit

Acronyms

BCR = blade count ratio $= N_{S1}/N_R$
CFD = computational fluid dynamics
FRAPP = fast response aerodynamic pressure probe
IGV = inlet guide vane

References

[1] Bellucci, J., Rubechini, F., and Arnone, A., 2015, "Some Experiences About the Impact of Unsteadiness in Turbine Flows," ASME Paper No. GT2015-43122.
[2] Pullan, G., 2006, "Secondary Flows and Loss Caused by Blade Row Interaction in a Turbine Stage," ASME J. Turbomach., **128**(3), pp. 484–491.
[3] Denton, J. D., 1993, "The 1993 IGTI Scholar Lecture: Loss Mechanisms in Turbomachines," ASME J. Turbomach., **115**(4), pp. 621–656.
[4] Chaluvadi, V. S. P., Kalfas, A. I., and Hodson, H. P., 2004, "Vortex Transport and Blade Interactions in High Pressure Turbines," ASME J. Turbomach., **126**(3), pp. 395–405.
[5] Venable, B. L., Delaney, R. A., Busby, J. A., Dorney, R. L., Dunn, M. G., Haldeman, C. W., and Abhari, R. S., 1999, "Influence of Vane–Blade Spacing on Transonic Turbine Stage Aerodynamics—Part I: Time-Averaged Data and Analysis," ASME J. Turbomach., **121**(4), pp. 663–672.
[6] Walraevens, R. E., Gallus, H. E., Jung, A. R., Mayer, J. F., and Stetter, H., 1998, "Experimental and Computational Study of the Unsteady Flow in a 1.5 Stage Axial Turbine With Emphasis on the Secondary Flow in the Second Stator," ASME Paper No. 98-GT-254.
[7] Ristic, D., Lakshminarayana, B., and Chu, S., 1999, "Three-Dimensional Flowfield Downstream of an Axial-Flow Turbine Rotor," J. Propul. Power, **15**(2), pp. 334–344.
[8] Gaetani, P., Persico, G., and Osnaghi, C., 2010, "Effects of Axial Gap on the Vane-Rotor Interaction in a Low Aspect Ratio Turbine Stage," J. Propul. Power, **26**(2), pp. 325–334.
[9] Pullan, G., and Denton, J. D., 2003, "Numerical Simulations of Vortex-Turbine Blade Interaction," 5th European Turbomachinery Conference, Prague, Czech Republic, Mar. 7–11.
[10] Yamada, K., Funazaki, K., Kikuchi, M., and Sato, H., 2009, "Influences of Axial Gap Between Blade Rows on Secondary Flows and Aerodynamic Performance in a Turbine Stage," ASME Paper No. GT2009-59855.
[11] Rubechini, F., Marconcini, M., Giovannini, M., Bellucci, J., and Arnone, A., 2015, "Accounting for Unsteady Interaction in Transonic Stages," ASME J. Eng. Gas Turbines Power, **137**(5), p. 052602.
[12] Arnone, A., 1994, "Viscous Analysis of Three-Dimensional Rotor Flow Using a Multigrid Method," ASME J. Turbomach., **116**(3), pp. 435–445.
[13] Spalart, P. R., and Allmaras, S. R., 1994, "A One-Equation Turbulence Model for Aerodynamic Flows," Rech. Aérosp., **1**, pp. 5–21306.
[14] Wilcox, D. C., 2008, "Formulation of the k–ω Turbulence Model Revisited," AIAA J., **46**(11), pp. 2823–2838.
[15] Menter, F. R., 1994, "Two–Equations Eddy Viscosity Turbulence Models for Engineering Applications," AIAA J., **32**(8), pp. 1598–1605.
[16] Arnone, A., Liou, M. S., and Povinelli, L. A., 1992, "Navier–Stokes Solution of Transonic Cascade Flow Using Non-Periodic C-Type Grids," J. Propul. Power, **8**(2), pp. 410–417.
[17] Arnone, A., Carnevale, E., and Marconcini, M., 1997, "Grid Dependency Study for the Nasa Rotor 37 Compressor Blade," ASME Paper No. 97–GT–384.
[18] Giovannini, M., Marconcini, M., Arnone, A., and Bertini, F., 2014, "Evaluation of Unsteady Computational Fluid Dynamics Models Applied to the Analysis of a Transonic High-Pressure Turbine Stage," Proc. Inst. Mech. Eng. Part A, **228**(7), pp. 813–824.
[19] Pacciani, R., Rubechini, F., Arnone, A., and Lutum, E., 2012, "Calculation of Steady and Periodic Unsteady Blade Surface Heat Transfer in Separated Transitional Flow," ASME J. Turbomach., **134**(6), p. 061037.
[20] Marconcini, M., Rubechini, F., Arnone, A., and Ibaraki, S., 2010, "Numerical Analysis of the Vaned Diffuser of a Transonic Centrifugal Compressor," ASME J. Turbomach., **132**(4), p. 041012.
[21] Bonaiuti, D., Arnone, A., Hah, C., and Hayami, H., 2002, "Development of Secondary Flow Field in a Low Solidity Diffuser in a Transonic Centrifugal Compressor Stage," ASME Paper No. 2002-GT-30371.
[22] Schmitt, S., Eulitz, F., Wallscheid, L., Arnone, A., and Marconcini, M., 2001, "Evaluation of Unsteady CFD Methods by Their Application to a Transonic Propfan Stage," ASME Paper No. 2001–GT–310.
[23] Marconcini, M., Rubechini, F., Arnone, A., Scotti Del Greco, A., and Biagi, R., 2012, "Aerodynamic Investigation of a High Pressure Ratio Turbo-Expander for Organic Rankine Cycle Applications," ASME Paper No. GT2012-69409.
[24] Rubechini, F., Marconcini, M., Arnone, A., Scotti Del Greco, A., and Biagi, R., 2013, "Special Challenges in the Computational Fluid Dynamics Modeling of Transonic Turbo-Expanders," ASME J. Eng. Gas Turbines Power, **135**(10), p. 102701.
[25] Wallis, A. M., Denton, J. D., and Demargne, A. A. J., 2001, "The Control of Shroud Leakage Flows to Reduce Aerodynamic Losses in a Low Aspect Ratio, Shrouded Axial Flow Turbine," ASME J. Turbomach., **123**(2), pp. 334–341.
[26] Pfau, A., Kalfas, A. I., and Abhari, R. S., 2007, "Making Use of Labyrinth Interaction Flow," ASME J. Turbomach., **129**(1), pp. 164–174.
[27] Rosic, B., Denton, J. D., and Curtis, E. M., 2007, "The Influence of Shroud and Cavity Geometry on Turbine Performance—an Experimental and Computational Study—Part 1: Shroud Geometry," ASME Paper No. GT2007-27769.
[28] Rosic, B., Denton, J. D., and Pullan, G., 2006, "The Importance of Shroud Leakage Modelling in Multistage Turbine Flow Calculations," ASME J. Turbomach., **128**(4), pp. 699–707.
[29] Rubechini, F., Marconcini, M., Arnone, A., Cecchi, S., and Daccà, F., 2007, "Some Aspects of CFD Modeling in the Analysis of a Low-Pressure Steam Turbine," ASME Paper No. GT2007-27235.
[30] Rubechini, F., Schneider, A., Arnone, A., Cecchi, S., and Garibaldi, P., 2012, "A Redesign Strategy to Improve the Efficiency of a 17-Stage Steam Turbine," ASME J. Turbomach., **134**(3), p. 031021.
[31] McGreeham, W. F., and Ko, S. H., 1989, "Power Dissipation in Smooth and Honeycomb Labyrinth Seals," ASME Paper No. 89-GT-220.
[32] Paradiso, B., Mora, A., Dossena, V., Gatti, G., Nesti, A., Arcangeli, L., and Maceli, N., 2015, "Flow Evolution in a One and a Half Axial Steam Turbine Stage Under Different Operating Conditions," ASME Paper No. GT2015-43201.
[33] Paradiso, B., Gaetani, P., Mora, A., Dossena, V., Osnaghi, C., Arcangeli, L., Gerbi, F., Maceli, N., and Quadrelli, R., 2015, "Design and Operation of a Low Speed Test Turbine Facility," 11th European Turbomachinery Conference, Madrid, Spain, Paper No. ETC2015-223.
[34] Persico, G., Gaetani, P., and Guardone, A., 2005, "Design and Analysis of New Concept Fast-Response Pressure Probes," Meas. Sci. Technol., **16**(9), p. 1741.
[35] Gaetani, P., Persico, G., Dossena, V., and Osnaghi, C., 2006, "Investigation of the Flow Field in a High-Pressure Turbine Stage for Two Stator-Rotor Axial Gap—Part II: Unsteady Flow Field," ASME J. Turbomach., **129**(3), pp. 580–590.
[36] Schennach, O., Woisetschlager, J., Paradiso, B., Persico, G., and Gaetani, P., 2009, "Three Dimensional Clocking Effects in a One and a Half Stage Transonic Turbine," ASME J. Turbomach., **132**(1), p. 011019.
[37] Cumpsty, N. A., and Horlock, J. H., 2006, "Averaging Nonuniform Flow for a Purpose," ASME J. Turbomach., **120**(1), pp. 120–129.
[38] Suresh, A., Hofer, D. C., and Tangirala, V. E., 2012, "Turbine Efficiency for Unsteady, Periodic Flows," ASME J. Turbomach., **134**(3), p. 034501.
[39] Van Zante, D. E., Chen, J. P., Hathaway, T. H., and Randall, C., 2008, "The Influence of Compressor Blade Row Interaction Modeling on Performance Estimates From Time-Accurate, Multistage, Navier–Stokes Simulations," ASME J. Turbomach., **130**(1), p. 011009.
[40] Sharma, O. P., Butler, T. L., Joslyn, H. D., and Dring, R. P., 1985, "Three-Dimensional Unsteady Flow in an Axial Flow Turbine," J. Propul. Power, **1**(1), pp. 29–38.
[41] Restemeier, M., Jeschke, P., Guendogdu, Y., and Gier, J., 2012, "Numerical and Experimental Analysis of the Effect of Variable Blade Row Spacing in a Subsonic Axial Turbine," ASME J. Turbomach., **135**(2), p. 021031.
[42] Dring, R. P., Joslyn, H. D., Hardin, L. W., and Wagner, J. H., 1982, "Turbine Rotor–Stator Interaction," ASME J. Eng. Power, **104**(4), pp. 729–742.